Development 130, 2139-2148
© 2003 The Company of Biologists Ltd
doi:10.1242/dev.00441

Isolation of *COV1*, a gene involved in the regulation of vascular patterning in the stem of *Arabidopsis*

Garry Parker[1], Rebecca Schofield[1], Björn Sundberg[2] and Simon Turner[1,*]

[1]School of Biological Sciences, The University of Manchester, 3.614 Stopford Building, Oxford Road, Manchester M13 9PT, UK
[2]Department of Forest Genetics and Plant Physiology, SLU, Umeå SE-901 83, Sweden
*Author for correspondence (e-mail: simon.turner@man.ac.uk)

Accepted 17 February 2003

SUMMARY

The molecular mechanisms that control the ordered patterning of vascular tissue development in plants are not well understood. Several models propose a two-component system for vascular differentiation. These components include an inducer of vascular tissue development and an inhibitor that prevents the formation of vascular bundles near pre-existing bundles. We have identified two recessive allelic mutants in *Arabidopsis*, designated *continuous vascular ring* (*cov1*), that display a dramatic increase in vascular tissue development in the stem in place of the interfascicular region that normally separates the vascular bundles. The mutant plants exhibited relatively normal vascular patterning in leaves and cotyledons. Analysis of the interaction of *cov1* with a known auxin signalling mutant and direct analysis of auxin concentrations suggests that *cov1* affects vascular pattering by some mechanism that is independent of auxin. The COV1 protein is predicted to be an integral membrane protein of unknown function, highly conserved between plants and bacteria. In plants, *COV1* is likely to be involved in a mechanism that negatively regulates the differentiation of vascular tissue in the stem.

Key words: *Arabidopsis*, Differentiation, Vascular bundle, Patterning, Auxin

INTRODUCTION

The vascular system in plants forms the structural architecture required to transport solutes and water. During primary vascular development, the pattern of vascular tissue is first visualised by the appearance of the procambial cells. These procambial cells subsequently differentiate into both the xylem and phloem that constitute each vascular bundle. Proper spatial arrangement of these vascular strands within the plant is essential for normal growth and development. The development of the vascular bundles occurs in a highly ordered and predictable pattern. However, the molecular regulation of this process remains poorly characterised.

In broad flat organs, such as leaves, the vascular tissue consists of an interconnected network that forms during the course of leaf development. By contrast, the pattern of primary vascular development in the stem is laid down in the region immediately below the apical meristem. The differentiation of vascular tissue is closely linked to the activity of the meristem. Early experiments demonstrated that the inductive effects of leaves and organ primordia on vascular development could be replaced by the application of auxin (Jacobs, 1952; Young, 1953). Many subsequent experiments have demonstrated the effect of auxin on both the induction and pattern of vascular tissue (for reviews, see Bennett et al., 1998; Berleth and Mattsson, 2000; Ye, 2002). A large number of experiments investigating vascular tissue induction by auxin were rationalised by Sachs (Sachs, 1981; Sachs, 1991), who suggested that the positive effects of high levels of auxin on the capacity for polar auxin transport (PAT) generate a positive feedback mechanism leading to the canalisation of auxin flow. The high levels of auxin in these regions result in vascular differentiation. Identification of the PIN1 protein has provided evidence to support the canalisation hypothesis. PIN1 is essential for PAT, and is normally localised on the basal membrane of the cell (Galweiler et al., 1998). During embryo development, transition from a uniform localisation of PIN to an orientated localisation occurs along the apical-basal axis, which is consistent with a positive feedback loop for auxin (Steinmann et al., 1999). Furthermore, disrupted localisation of PIN1 in *emb30*/*gnom* mutants results in a proliferation of vascular tissue that is consistent with auxin delivery to inappropriate cell types (Koizumi et al., 2000; Steinmann et al., 1999).

A large number of experiments by Sachs suggested that auxin may also play a role in the inhibition of vascular bundle development. Pre-existing vascular bundles with high rates of auxin transport inhibited the development of new vascular strands in their immediate vicinity (Sachs, 1981; Sachs, 1991). Interestingly, recent experiments by Reinhardt et al. (Reinhardt et al., 2000) suggest that auxin is involved in both inductive and inhibitory affects in organ formation. Although auxin is able to induce primordia formation, once formed, the region adjacent to these primordia becomes insensitive to further

auxin application. The mechanism by which auxin, or some other signalling molecule from the developing primordia, exerts this inhibitory effect remains unclear.

Isolation of mutants that contain islands of vascular tissue that are not connected to the existing vascular tissue are harder to reconcile with the canalisation hypothesis (Carland et al., 1999; Deyholos et al., 2000; Koizumi et al., 2000). Some of these mutants have normal responses to auxin and may be explained more easily by the diffusion-reaction pre-pattern hypothesis. Based on computer modelling, the diffusion-reaction hypothesis proposes the interaction of two diffusible substances with varying diffusion rates that regulate the autonomous formation of veins in an initially uniform field. One of these substances promotes the induction of vascular tissue, whereas the other results in inhibition of vascular development (Koch and Meinhardt, 1994). Although there is a good deal of evidence to support the inductive effects of auxin on vascular development, there is little evidence on what the inhibitory element might be.

In wild-type *Arabidopsis* stems, the pattern of vascular bundles is very ordered with five to eight bundles developing around the stem, separated by the interfascicular regions. However, the molecular mechanisms that control this patterning remain unclear. There are a limited number of mutants available that show altered vascular patterning in the stem. The *amphivasal vascular bundle* (*avb*) mutant (Zhong et al., 1999) has an increased number of vascular bundles in the stem, many of which are abnormally localised in the pith. The vascular bundles also show an amphivasal pattern with the phloem surrounded by xylem. Another mutant, *acaulis5* (*acl5*) (Hanzawa et al., 1997), has vascular bundles that are surrounded by an abnormally extended sheath of cells with thickened walls. Although the number of veins in *acl5* plants is similar in wild-type plants, the amount of differentiated vascular tissue within the vascular bundles appears to be greater in the mutant.

In this study, we report the cloning of a gene involved in maintaining the ordered patterning of vascular bundles within the stem of *Arabidopsis*. Mutations in this gene lead to disruptions in the patterning of differentiated vascular tissue in the stem, resulting in a continuous ring-like pattern of xylem and phloem, with very little interfascicular tissue and the loss of defined vascular bundles. Based on the phenotype of the vascular tissue in the stem, this mutant was designated *continuous vascular* (*cov1*). COV1 is predicted to be an integral membrane protein that may be involved in the perception or transport of a signalling molecule that negatively regulates the differentiation of vascular tissue in the developing stem of *Arabidopsis*.

MATERIALS AND METHODS

Plant growth conditions and mutant scoring

Seeds were sterilised by washing for 10 minutes in sterile water containing 10% bleach and 0.01% Triton X-100, followed by five washes with sterile water. The seeds were then imbibed in 0.1% agar for 48 hours at 4°C. Seeds were germinated on plates containing Murashige and Skoog medium (MS) (4.4 g/l) (Sigma), MES buffer (0.5 g/l) (Sigma) and 1% agar. Plates were placed in a growth cabinet under continuous light at 22°C. Once the seedlings had germinated, they were transferred to pots containing a commercial compost/perlite/vermiculite mixture and grown under continuous light at 22°C in growth chambers. Mutant alleles were identified from a screen of ethyl methane sulphonate (EMS)-mutated M2 seed of wild-type L*er*. Scoring was performed by taking hand-cut cross-sections of the base of stems from 4-week-old plants. Sections were stained either with 0.05% Aniline Blue (0.67 M phosphate buffer; pH 8.0) and observed using UV microscopy, or with 0.02% Toluidine Blue and observed using brightfield microscopy.

DNA and RNA isolation

DNA was isolated from an F_2-mapping population as described by Guidet et al. (Guidet et al., 1991). The testcross population was screened using an alternative rapid DNA extraction procedure. Small sections (6-9 mm^2) of the cotyledons or first emerging leaves of young seedlings were removed and ground in 20 μl 0.25 M NaOH. Grinding was performed in 96-well PCR plates using plastic pipette tip ends sealed by passing them through a flame. Once the tissue was homogenised, 7 μl of the sample was removed and added to 150 μl 0.3 M Tris-HCl buffer (pH 8.0). Each PCR reaction used 7 μl of this mix, in a total volume of 20 μl. RNA extraction was performed using an RNeasy Plant Mini Kit (Qiagen), and RNA was quantified on a BioSpec-1601 E spectrophotometer (Shimadzu). A full-length cDNA (wild-type Columbia) of *COV1* was obtained from a library generated by Asamizu et al. (Asamizu et al., 2000), and also by RT-PCR analysis from wild-type L*er*.

PCR and RT-PCR

PCR was performed in a PTC100 thermal cycler (MJ Research) using Taq polymerase (Life Technologies). Each reaction was performed in a total volume of 25 μl, containing 100 ng DNA with 50 mM KCl, 10 mM Tris-HCl (pH 9.0), 0.1% Triton X-100, 200 μM dNTPs (each), 1.5 mM $MgCl_2$, 0.5 units Taq polymerase and 1 μM each primer. PCR conditions were as follows: 94°C for 2 minutes; 35 cycles of 94°C for 30 seconds, 55°C (variable between primer pairs) for 30 seconds and 72°C for 60 seconds; and 2 minutes at 72°C. RT-PCR was performed using a One-Step RT-PCR Kit (ABgene) in a volume of 50 μl with 1 μg of total RNA. Gene-specific primers were used for amplification. PCR conditions were as follows: 47°C for 30 minutes; 94°C for 2 minutes; 35 cycles of 94°C for 20 seconds, 55°C for 30 seconds and 72°C for 90 seconds. The positive control (MS2) was provided with the kit. All PCR products were run on 1-2% agarose gels in TBE buffer and visualised using ethidium bromide staining.

DNA sequencing

Templates generated from restriction fragment cloning, PCR and RT-PCR were gel purified using a High Pure PCR Product Purification Kit (Roche), and cloned into the vector pGEM-T Easy (Promega) for sequencing. Specific primers were designed and synthesised (MWG Biotech) for use along with vector specific T7 and SP6 primers. Plasmid templates were prepared using a QIAprep Spin Miniprep Kit (Qiagen), and sequencing reations were performed using an ABI Prism Sequencing Kit (Applied Biosystems). Sequence data were analysed using the ContigExpress program (InforMax). Sequences used for alignment were identified from BLAST searches of GenBank. Alignments were carried out using CLUSTAL W (Thompson et al., 1994).

Expression analysis

Expression analysis was performed using real-time quantitative PCR (qPCR). Primers and probes were designed for the various genes using Primer Express (v1.0) (Applied Biosystems), and probes were labelled with 6-FAM (FAM; 5′) and tetramethylrhodamin (TAMRA; 3′). First strand synthesis was performed in a volume of 20 μl, containing 1 μg total RNA with 500 ng poly-(dT) primer and 100 U reverse transcriptase (Promega), at 42°C for 60 minutes. PCR conditions were as follows: 50°C for 2 minutes; 95°C for 10 minutes;

40 cycles of 95°C for 15 seconds and 60°C for 60 seconds. PCR reactions were performed in a volume of 25 μl, containing 12.5 μl 2× qPCR Mastermix (Eurogentec), 5 pmol probe and 25 pmol each primer. Data analysis was carried out using the Sequence Detector (v1.7) program (Applied Biosystems).

Complementation

DNA fragments containing genes of interest were subcloned into the binary vector pc2300 (Cambia) for complementation purposes. Complementation was carried out by transforming plants using *Agrobacterium tumefaciens* (GV3101) containing various constructs described by Bent and Clough (Bent and Clough, 1998). Transformants were identified by growing seed of the transformed plants on agar plates containing MS (2.2 g/l) and the appropriate selection antibiotic. After 2 weeks, the resistant seedlings were transplanted into pots and grown to maturity to determine their phenotype.

Auxin experiments

Endogenous auxin levels were quantified by gas chromatography-selected ion monitoring-mass spectrometry with 13C6IAA as an internal standard, as described by Edlund et al. (Edlund et al., 1995). To determine response to auxin, seedlings were grown on MS agar plates containing various levels of 2,4-Dichlorophenoxy-acetic acid (2,4-D; 0.05, 0.1 and 0.25 μM), in a vertical position in a growth cabinet under continuous light at 22°C.

RESULTS

Phenotype and description of the mutant

From a screen of ~5000 EMS-mutagenised M2 Landsberg *erecta* (L*er*) plants, two lines were isolated from independent seed batches that exhibited altered patterns of vascular bundle spacing. These two mutant lines were shown to be allelic by reciprocal crossing and subsequent scoring of the F_1 plants, whereby all plants scored were found to exhibit the mutant phenotype. These mutants were named *continuous vascular ring* (*cov1*), and the two lines designated *cov1-1* and *cov1-2*. The heterozygous plants for both mutant alleles show normal vascular patterning in the stem and the mature plants are indistinguishable from wild-type L*er*, indicating that the mutation is fully recessive. An F_2 population generated from a cross of *cov1-1* back to the L*er* parent yielded 57 wild-type plants and 22 *cov1* plants, which fits the expected 3:1 hypothesis (χ^2=0.34, P=0.47) for a single nuclear recessive mutation.

Cross-sections of mature 4-week-old inflorescence stems showed that both alleles had a significant defect in the patterning and development of the vascular bundles compared with wild-type L*er* (Fig. 1). In wild-type L*er* plants, six to eight vascular bundles develop in a very ordered and predictable pattern around the stem, with bundles of phloem and xylem separated by interfascicular regions made up of differentiated fibres. However, in the *cov1* mutants, the ordered patterning of vascular bundles is lost and is replaced by an almost continuous ring of both phloem and xylem tissue around the whole stem. This increase in vascular tissue appears to replace the area normally occupied by the interfascicular cells such that, in plants exhibiting a severe mutant phenotype, the interfascicular region was virtually absent or significantly reduced (Fig. 1). This proliferation of vascular tissue is also accompanied by a reduction in stem thickness.

In order to study further the development of the vascular bundles in the stem of wild-type L*er* and *cov1-1* plants, cross-sections of 4-week-old plants were taken at various positions along the inflorescence stem to observe the vascular phenotype. Sections were taken just below the apex, a quarter of the way down the stem and half way down the stem (Fig. 2). The results showed that directly below the apical meristem, wild-type plants exhibit a clearly defined pattern of vascular bundles containing both xylem and phloem (Fig. 2). Corresponding bundles are also visualised in *cov1-1* plants (Fig. 2). However, in the *cov1-1* mutant there was clear evidence of additional differentiation of vascular tissue in the region normally occupied by interfascicular cells. This differentiation is clearly visible as brightly stained yellow phloem cells in between, and

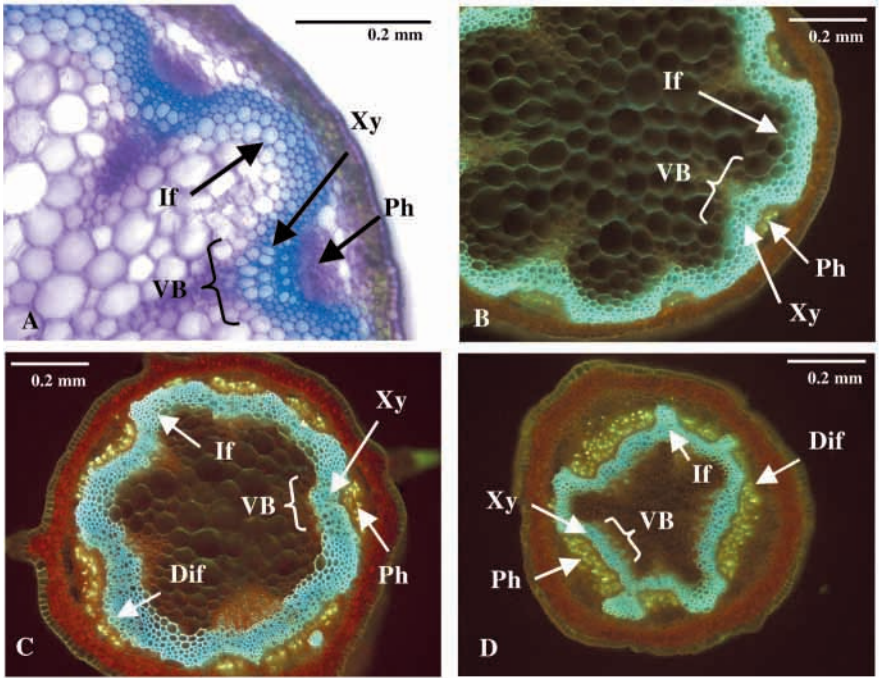

Fig. 1. Hand-cut sections of stems from wild-type (A,B), *cov1-1* (C) or *cov1-2* (D) plants stained with Toluidine Blue and viewed under brightfield illumination (A), or stained with Aniline Blue and viewed under UV light (B-D). Xylem and interfascicular cells are identified by their blue-stained walls when stained with Toluidine Blue, or by their blue fluorescence when stained with Analine Blue. Phloem cells produce a distinctive yellow fluorescence when stained with Analine Blue. VB, vascular bundle; Ph, phloem; Xy, xylem; If, interfascicular region; Dif, differentiation in the interfascicular region.

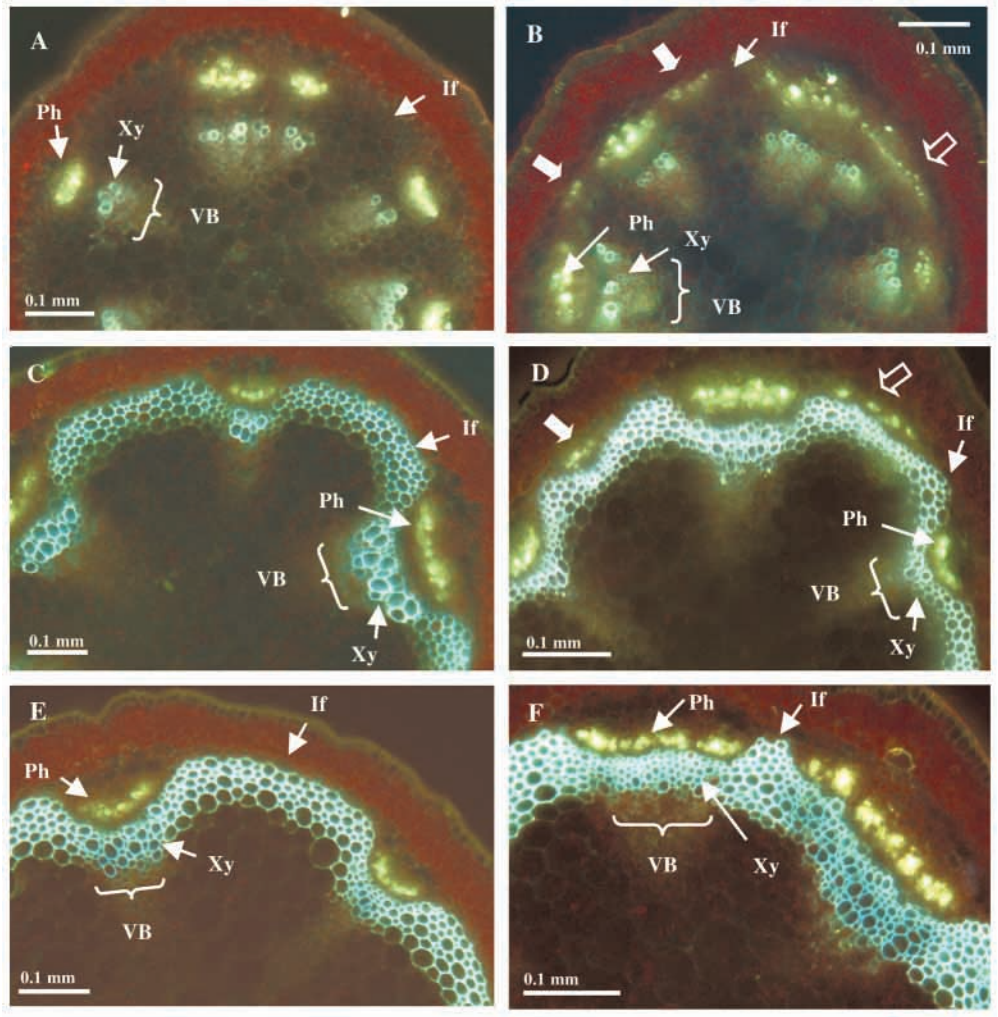

Fig. 2. Hand-cut sections from wild-type (A,C,E) and *cov1-1* (B,D,F) plants. Sections were taken from four-week-old plants at different positions down the stem: just below the apical meristem (A,B); a quarter of the way down (C,D); and halfway down (E,F). Sections were stained with Aniline Blue and viewed under UV light. Additional differentiation of vascular bundles in the interfascicular region and unconnected to the normally patterned vascular bundles can be seen in the *cov1-1* sections (thick white arrows in B,D). There is also evidence of lateral expansion of vascular bundles or additional differentiation of vascular tissue in close proximity to the normally patterned vascular bundles (open arrows in B,D). VB, vascular bundle; If, interfascicular region; Ph, phloem; Xy, xylem.

unconnected to, the vascular bundles, which exhibit a more normal pattern of development (Fig. 2). It can also be seen that additional differentiation occurs directly adjacent to the developing vascular bundles (Fig. 2). It is unclear at present whether this is actually lateral expansion of the established vascular bundle or the initiation of additional differentiation in the region immediately adjacent to the pre-existing vascular bundle. This patterning, though somewhat variable, continues down the stem such that, at the base, an almost continuous ring of differentiated vascular tissue is visible (Fig. 1).

Under the conditions in which these plants were grown, no evidence of any secondary growth was observed either in the wild type or in the mutant. Although both alleles show similar phenotypes, the second allele (*cov1-2*) is generally more severe (Fig. 1). Cross-sections of the hypocotyl were also compared between mutant and wild-type plants, and the patterning in this region of the plants appeared to be similar (data not shown). The *cov1* mutants were slower growing and shorter compared with wild-type L*er* plants. At flowering, *cov1-1* was approximately two thirds the height of wild-type L*er* and *cov1-2* was less than half the height of wild-type L*er* when grown under continuous light (Fig. 3). Electron microscopy studies of stems from *cov1-1* and wild-type plants showed that the cells in the mutant stems were shorter and smaller compared with wild-type L*er* (data not shown), but the number of internodes is similar. The siliques of *cov1* were shorter and more wrinkled compared with wild-type L*er*, and both alleles showed a variable slightly twisted leaf phenotype, with *cov1-2* being more severe in both respects.

Leaves and cotyledons from wild type and both mutant alleles were cleared to observe the vein pattern and to determine the cause of the twisted leaf phenotype. These results showed that there was no difference in vein patterning in cotyledons (data not shown), and that the patterning of primary, secondary and tertiary veins in leaves was similar between wild-type and mutant plants (Fig. 3). However, the shape of the leaves in both mutant alleles appeared to be somewhat asymmetric compared with wild type. This asymmetry, although minor, may give rise to the visible twisted leaf phenotype. There were no apparent defects in phyllotaxis in either of the mutant alleles. When grown on agar plates, the roots were slower growing and shorter in both mutant alleles, but there was little difference in numbers of lateral roots compared with wild-type L*er*. There was no difference in the phenotype of etiolated seedlings of *cov1-1* and wild-type plants when germinated in the dark (data not shown).

Mapping the *cov1* gene

An initial F_2-mapping population of 600 plants was generated from a cross between *cov1-1* and wild-type Columbia plants.

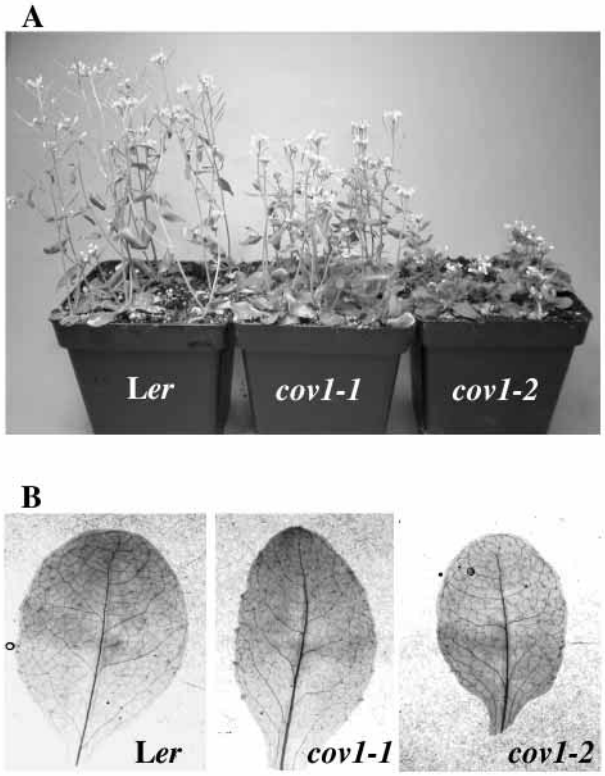

Fig. 3. (A) Wild-type, *cov1-1* and *cov1-2* plants were grown side by side under continuous light and photographed at four weeks of age. (B) Although the leaves of both mutant alleles showed a wrinkled phenotype, the vein patterning was similar to wild-type though slightly asymmetric in both *cov1-1* and *cov1-2*.

The population was scored for the mutant phenotype, and 120 mutant plants were selected and screened with polymorphic microsatellite (SSLP) markers spanning all five chromosomes. Linkage was identified with markers on the long arm of chromosome 2. Further SSLP markers were generated in this region for more detailed mapping and the gene was localised to a region of ~500 kb. Polymorphic co-dominant markers located on BACs F27F23 (SSLP33) and F21P24 (SSLP23), which were suitable for rapid PCR screening, were identified that flanked a region of ~2 Mb containing the *COV1* gene. These markers were used to screen a testcross population to identify critical recombinants in this region. The testcross population was generated by crossing F_1 plants generated from the initial cross with Columbia back to *cov1-1* to generate a population that was 50% mutant and 50% wild type (heterozygous). Out of 2148 testcross plants screened, 105 showed recombination between the two flanking markers. These critical recombinants were used to finely map the gene further using additional SSLP and cleaved amplified polymorphic sequence (CAPS) markers generated on each of the BACs spanning this region. Based on the mapping data obtained from these plants, the gene was placed within a region of 77 kb, spanned by the ends of two adjacent BACs (T2G17 and F11A3) (Fig. 4).

Cloning and complementation

The two BACs spanning the region to which the gene had been mapped were digested using three restriction enzymes (*Sac*I, *Sal*I and *Xho*I) and the fragments subcloned into a binary vector for *Agrobacterium*-mediated transformation. Partial complementation [100% *cov1-1* plants (n=30) and 68% *cov1-2* plants (n=34)] was achieved when mutant plants were transformed with an 11,644 bp *Sac*I fragment, pGDP1 (Fig. 4), that contained four predicted genes. Sequence analysis of the whole fragment from mutant plants did not identify any mutations when compared with wild type. Complementation of *cov1-1* was also achieved with a 10,599 bp *Xho*I/*Sal*I

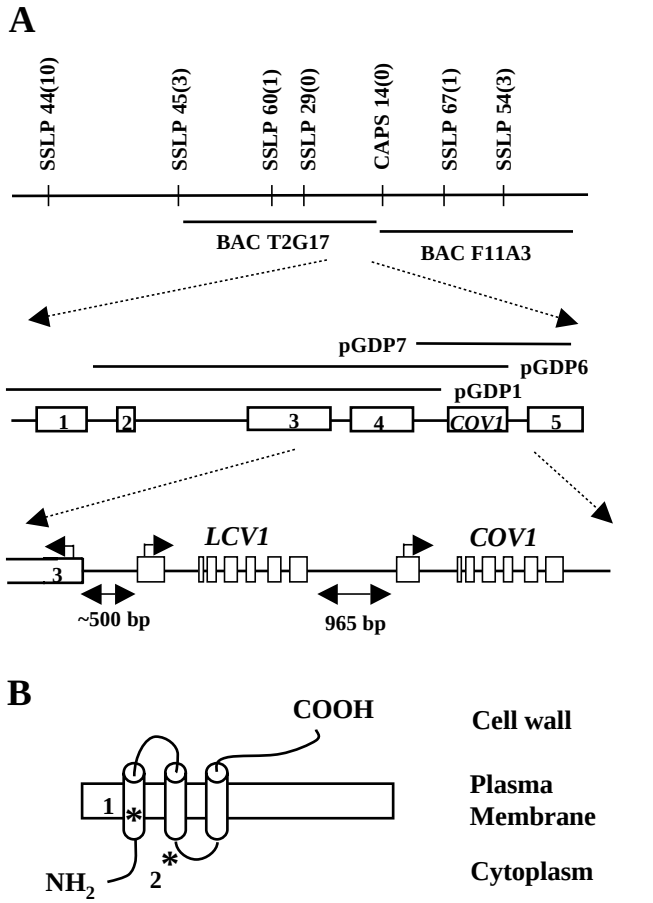

Fig. 4. (A) Map-based cloning of *COV1* based on data obtained from recombinants identified in the testcross screen. The number of recombinants identified between *COV1* and closely linked markers are shown in brackets. Subclones used to determine complementation are shown as unbroken black lines. The *cov1-1* mutant was partially complemented with pGDP1 and fully complemented with pGDP6 and pGDP7. Other genes in the region are indicated by numbers (1, At2g20160; 2, At2g20150; 3, At2g20140; 4, At2g20130; 5, At2g20110). The intron-exon structure and position of *COV1* and the closely related gene *LCV1* are also shown (bottom). The predicted translation initiation sites are indicated by arrows. (B) The predicted topology of COV1. The protein contains three predicted membrane-spanning domains; the N-terminal end of the protein is predicted to be intracellular and the C-terminal end is predicted to be in the wall. The mutation in *cov1-1* (*1) is in exon 3, which forms part of the first membrane-spanning domain and results in an amino acid change from proline to serine ($P^{76}\rightarrow S$). The mutation in *cov1-2* (*2) is located in exon 4, which is predicted to lie just after the second membrane domain and results in an amino acid change from glycine to arginine ($G^{130}\rightarrow R$).

fragment, pGDP6, which also contained four predicted genes, including three of the genes found on pGDP1 and an additional predicted gene (GenBank Accession Number At2g20120). This gene was isolated independently on a 5722 bp *Bst*UI fragment, pGDP7, that contained only a single complete predicted gene (At2g20120). Transformation of *cov1-1* plants with pGDP7 restored both the vascular phenotype and the growth phenotypes (Fig. 5). This fragment was also able to complement the *cov1-2* allele, with all transformed plants (n=10) showing wild-type vascular patterning in the stem (data not shown).

Comparison of the DNA sequencing of pGDP6 from wild-type L*er* and *cov1-1* identified a single base-pair mutation in At2g20120. Comparison of the *cov1-2* sequence with wild type also revealed the presence of a single base-pair change in this open reading frame. Consequently, both complementation and sequence analysis demonstrated that the *cov1* mutation is the result of a defect in At2g20120 (from hereon referred to as *COV1*).

A full-length EST cDNA clone of At2g20120 (*COV1*) from a Colombia background was obtained (Asamizu et al., 2000) and the DNA sequence deposited in GenBank (Accession Number AY170845). RT-PCR was performed using mRNA from wild-type L*er*, and the coding sequence was identical to the cDNA clone from Columbia. Comparison of the cDNA and genomic sequence revealed that the *COV1* gene comprises seven exons and six introns (Fig. 4). The mutation in *cov1-1* is located in the third exon (C→T) and results in an amino acid change from proline to serine (P^{76}→S). In *cov1-2* the mutation occurred in the fourth exon (G→A) and results in an amino acid change from glycine to arginine (G^{130}→R). The full-length protein is predicted to be 268 amino acids in length, although there are two possible in frame start codons (Fig. 6) and it is unclear which one is used. The predicted structure of the gene indicates that the N-terminal end of the protein is cytoplasmic, followed by three membrane spanning domains with the C-terminal end predicted to be in the wall (Fig. 4). The mutation in the *cov1-1* allele is located in the first membrane spanning domain, whereas the mutation in *cov1-2* is located intracellularly, just after the second predicted membrane spanning domain. Based on phenotype, the mutation in *cov1-2* is more severe and causes a greater loss of function of the protein, as evidenced by the extreme dwarf growth habit and increased disruption of the vascular patterning in the stem.

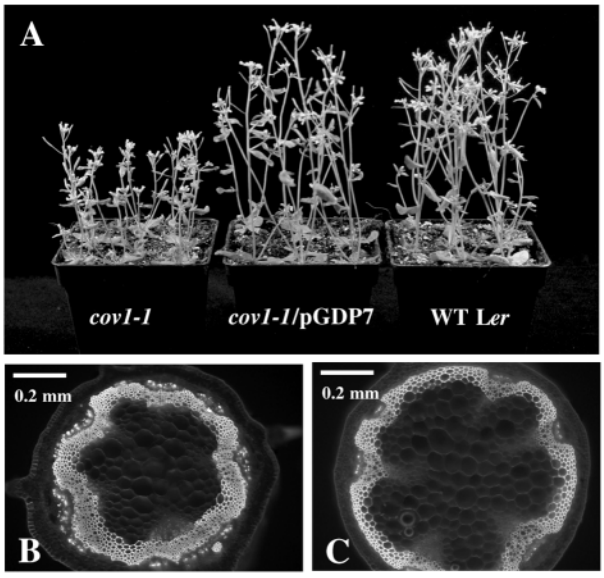

Fig. 5. (A) Morphology of four-week-old plants of *cov1-1*, *cov1-1* transformed with pGDP7 and wild-type L*er* grown side by side, demonstrating that pGDP7 complements the mutation. Sections from the base of the stem of a four-week-old *cov1-1* plant (B) and a *cov1-1* plant transformed with pGDP7 (C), stained with Aniline Blue and viewed under UV light. In both A and C, *cov1-1* plants transformed with pGDP7 are indistinguishable from the wild type.

Analysis of the genome revealed that there are three other related genes in *Arabidopsis*. These genes have been designated *LIKE COV* (*LCV*). *LCV1* (GenBank Accession Number At2g20130; 238 amino acids) lies directly upstream (~1 kb) of *COV1* (Fig. 4) and is almost identical at the amino acid level (95%), which indicates that it may be a recent duplication (Fig. 6). *LCV2* (GenBank Accession Number At1g43130; 261 amino acids) is located on chromosome 1 and also has a high level of homology at the protein level to *COV1* (58% identity); the most variable region is at the 5′ end, which is predicted to be cytoplasmic. *LCV3* (GenBank Accession Number At2g18460; 129 amino acids) is located on chromosome 2 and, although being closely related (52% identity), is truncated relative to *COV1* and exhibits homology to only the carboxy-half of COV1. EST sequences are available for all four members of the family, which suggests that they are all expressed.

Analysis of protein sequences from other genomes has revealed that there is a homologous gene to *COV1* in rice, with the predicted sequence from a cDNA exhibiting 59% identity to COV1 (Fig. 6). *COV1* also has clear homologues in a large number of bacterial genomes. Alignment with two of these bacterial sequences, from *Mesorhizobium loti* and *Agrobacterium tumefaciens*, is shown in Fig. 6. They both exhibit sequence conservation with COV1 along their entire length. All of the related bacterial genes are annotated as membrane proteins of unknown function. These results indicate that these genes may be involved in cellular mechanisms that are specific to plants and bacteria, and that the *COV1* gene may play a common role within these organisms.

Expression of *COV1* and *LCV1*

RT-PCR experiments demonstrate that the *COV1* gene is alternatively spliced in both wild-type L*er* plants and the two mutant alleles (data not shown). Sequence analysis revealed that the alternatively spliced product was the result of the retention of intron 2, which leads to a premature stop codon and a truncated protein. Real-time quantitative PCR (qPCR) analysis was carried out to determine the relative levels of the different transcripts in wild-type and mutant plants. In wild-type L*er* and *cov1-2* plants, the amount of alternatively spliced product compared with the correctly spliced product was 0.95%, but in the *cov1-1* mutant plants, this was increased to 2.01% (data not shown). Because of the high degree of similarity between *COV1* and the three related genes, qPCR was used to determine the expression levels of the specific genes in various plant tissues. The results of the qPCR

```
COV1              1 MGDEKPVIVMANRERDRELLLIPVADSGDKDDGSSSKPSSSSSASSSSHQSSHETLSLFI
LCV1              1 ---------MANRERDRELLLIPVADFGDKDDGSSSKPSSSSSASSS-HQSGHETLSLFI
Oryza             1 ---------MAEKEESTSIPLSQAAEAVDPEDPAKSPPRPSSPTISST-----RKACCAVL
Mesorhizobium     1 ---------------------------------MSDAP-KTSGMIR-------------L
Agrobacterium     1 ---------------------------------MTDIPVKISFAAR-------------L

COV1             60 RGWASKKFMTGCVILLPIAITFYITWWFIHFVDGFFSPIY-------AQLGINVFGFGFL
LCV1             50 RGWASKKFMTGCVILLPIAVTFYTTWWFIHFVDGFFSPIY-------ALLGINIFGFGFL
Oryza            47 QSWVSRKFMTGCVVLFPVAVTFFITWWFIQFVDGFFSPLY-------AKLGIDIFGLGFL
Mesorhizobium    14 R----NYFLTGFVVCAPLAITAYIAWSFIGWVDSWVKPYIPARYSPDTYLPFPVPGFGLI
Agrobacterium    15 R----NSFLTGVLILAPVTIIMWLVWSFLQWADSWVKPYIPARYDPEQYFDVAIPGFGLL

COV1            113 TSIAFIFLVGVFMSSWLGASVLNLGEWFIKRMPFVRHIYNASKQISTAISPDQNTQAFKE
LCV1            103 TSIAFIFLVGVFMSSWLGASVLNLGEWFIKRMPFVRHIYNASKQISTAISPDQNTQAFKE
Oryza           100 TSLVFIFLVGIFVSSWVGSTIFWVGEWFIKKMPFVRHIYSASKQVSTAISPDQNTTAFKE
Mesorhizobium    70 VALILITLIGFLTANIVGRAIVGFGERLLGRMPLVRGIYGSLKQIFEAVLSNK-GDMFRQ
Agrobacterium    71 IAVIGITLIGFLGNNLIGKWIVGVGESVLNRMPLVRPIYKSIKQLFESVLKEH-SNSFKK

COV1            173 VAIIRHPRVGEYAFGFITS----TVVLQNYPTEEELCCVYVPTN-HLYIGDILLVNSNDV
LCV1            163 VAIIRHPRVGEYAFGFITS----TVVLQNYPTEEELCCVYVPTN-HLYIGDILLVNSNDV
Oryza           160 VAIIRHPRIGEYAFGFITS----TVVLQTDKGDEELCSVYVPTN-HLYIGDIFLVNSEEI
Mesorhizobium   129 VGLVEYPRKGVWSLVFVASEKETEINEKLDQEGDPLIAVFMPCTPNPTTGFLMYVLKSDI
Agrobacterium   130 VGLIEFPSSGTWAMVFVSSEVKGELAHRFNEMGQQMVAVFLPPTPVPTAGFLLFVPKDKI

COV1            228 IRPNLSVREGIEIVVSGGMSMPQILSTVD-K---PLAS------------IDRATSL--
LCV1            218 IRPNLSVREGIEIVVSGGMSMPQILSTLD-K---PLAS------------IGNES----
Oryza           215 IRPNLSIREGIEIIVSGGMTMPQVIASLEPT---PRKSQNI---------RLNRIMI----
Mesorhizobium   189 VLLDMTIEDGAKLIVSAGLVAPEVKSKWVTLNGEPINGTVANPPLGSHPARRSRTASSRP
Agrobacterium   190 VMLDMTPEDAAKLLISGGLVAPDFTPPKVIA---PV-----------------------
```

Fig. 6. Comparison of COV1 with its closest homologue in *Arabidopsis* (LCV1) and homologues from rice and two bacterial species (*Mesorhizobium loti* and *Agrobacterium tumefaciens*). Black boxes indicate regions in which more than half the residues are identical and grey boxes indicate conserved residues. Dashes have been introduced to optimise the alignment.

experiments showed that *COV1* was highly expressed in flowers and stems; a reasonable level of expression was also seen in roots, but less in leaves (Fig. 7). The expression levels of *LCV1* were also measured and were found to be much lower than those of *COV1*.

Response to auxin and auxin levels

To determine whether mutant plants showed an altered response to auxin, seedlings of wild-type L*er* and mutant *cov1-1* plants were germinated and grown on MS agar plates containing different concentrations of 2,4-D (0.1 μM, 0.25 μM and 0.5 μM). The results showed that there was no difference in root growth between *cov1-1* and wild-type L*er* in response to auxin (Fig. 8). In addition, *cov1-1* produced wild-type

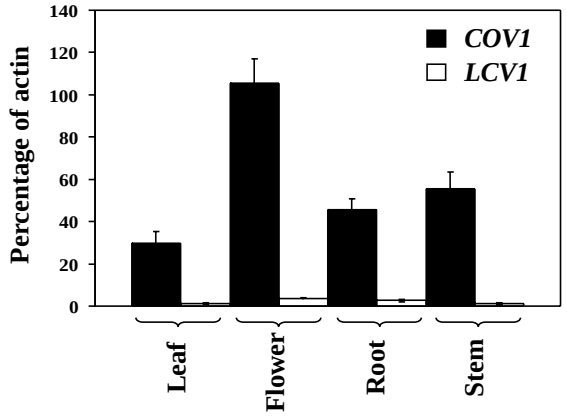

Fig. 7. *COV1* is expressed in all tissues and at a much higher level than *LCV1* (*n*≥3). The expression levels of *COV1* and *LCV1* in various tissue was determined using quantitative PCR and are presented as a percentage of the actin control. Values are mean±s.e.m.

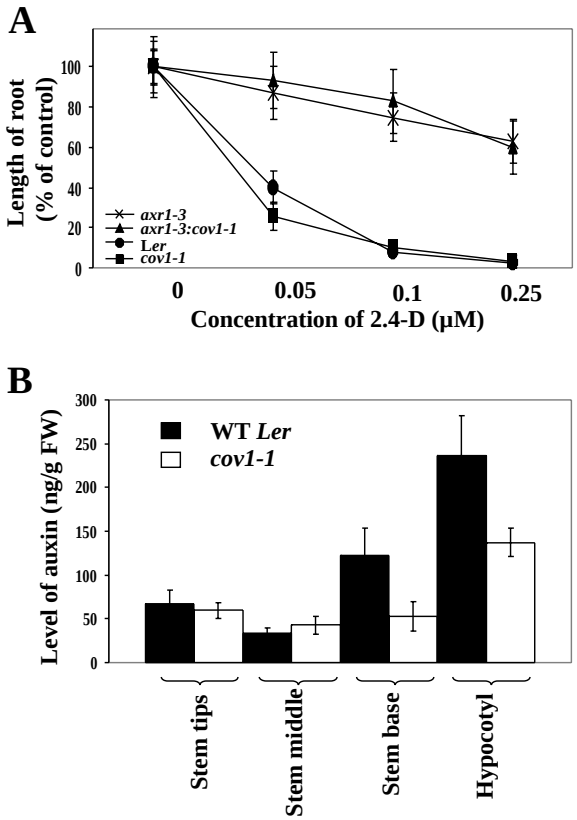

Fig. 8. (A) wild-type L*er*, *cov1-1*, *axr1-3* and *cov1-1:axr1-3* double mutant plants were grown vertically on agar plates containing increasing concentrations of 2,4-D; root lengths were measured after 7 days (*n*≥12). (B) Auxin levels were measured in various regions of the inflorescence stems of wild-type L*er* and *cov1-1* plants (*n*≥3). The only regions where there were significant differences were in the base of the stems and in the hypocotyl.

numbers of root hairs and exhibited a normal gravitropic response (data not shown).

Double mutants were generated between *cov1-1* and *axr1-3*: a mutant known to be defective in almost every measurable aspect of auxin signalling (for a review, see Kepinski and Leyser, 2002) and which is resistant to auxin (Lincoln et al., 1990). The double mutants did not show a significantly different plant phenotype compared with either *cov1-1* or *axr1-3* mutant plants. The *cov1-1:axr1-3* plants grew to a similar height compared with *cov1-1*, and exhibited the disrupted vascular patterning in the stem characteristic of *cov1-1* (data not shown). The double mutants were grown on various concentrations of 2,4-D and their root lengths were measured. Both the *axr1-3* and *cov1-1:axr1-3* double mutants were equally resistant to auxin compared with wild-type L*er* and *cov1-1* plants (Fig. 8). The double mutant showed no significant alteration in its response to 2,4-D compared with the single *axr1-3* mutant. Overall the results indicate that the double mutants were not more resistant to 2,4-D than was the *axr1-3* mutant, which suggests that *COV1* does not act in the same signalling pathway as *AXR1*.

To determine whether there was any difference in auxin concentration between wild-type L*er* and *cov1-1* mutant plants, levels of auxin were measured at various positions along the inflorescence stem. These included the region just below the apical meristem; half way down the stem; at the base of the stem; and in the hypocotyl. The results of the analysis showed that there was no significant difference in auxin concentration in the upper part of the stem (Fig. 8). However, in the base of the stem and in the hypocotyl there was a significant difference: wild-type plants contained almost twice the amount of auxin as did *cov1-1* plants.

cov1-1 plants were also transformed with a construct containing the auxin inducible *IAA2* promoter coupled with the β glucuronidase (GUS) reporter gene as an indicator of the presence of auxin (Swarup et al., 2001). Transformed *cov1-1* plants were then crossed with wild-type L*er* plants for comparison, to reduce any variation caused by positional effects. There was little difference in expression patterns of GUS between the wild-type or *cov1-1*-mutant plants in either the seedlings or developing stems (data not shown), which indicates that there was no difference in the distribution of auxin in the upper part of the stem. There was no detectable IAA2-GUS expression at the base of the stem in either wild-type L*er* or *cov1-1*-transformed plants where the auxin measurements identified a significant difference between wild-type and mutant plants.

DISCUSSION

cov1 is a novel mutation in which there is a large alteration in the pattern of vascular tissue in the stem. The positioning of the vascular tissue around the outside of the pith is normal, but the vascular tissue proliferates at the expense of the interfascicular tissue that normally separates each vascular bundle (Fig, 1). Distinct vascular bundles are clearly visible close to the apex early in development; however, in contrast to wild type, additional vascular tissue is clearly visible between the newly forming bundles in *cov1* mutants (Fig. 2). This apparent additional recruitment of new bundles represents the development of vascular tissue unconnected to existing vascular bundles. In addition, vascular tissue also develops adjacent to existing vascular bundles. It is unclear whether this represents the expansion of existing vascular bundles or the formation of new vascular tissue that coincidently adjoins an existing strand. In the mutant, vascular development continues such that, in some mature stems, the interfascicular regions are almost absent (Figs 1, 2). However, *cov1-1* and *cov1-2* mutant plants do not show any significant defects of vascular patterning in cleared cotyledons or leaves compared with wild type, although the shape of the leaves in both mutant alleles appeared to be slightly asymmetric (Fig. 3), which is thought to give rise to the slightly twisted leaf phentotype. In general, leaf shape mutants show pattern defects in the number and placement of the major veins (Dengler and Kang, 2001) but these appear to be relatively normal in the *cov1* mutants. The fact that any defects in the patterning of veins in leaves were minor compared with the disruption of vascular patterning observed in the stem suggests that vascular differentiation in leaves and stems may, at least in part, be regulated by different pathways. This idea is supported by the recent description of a number of mutants that show altered patterns of vascular development in the cotyledons and leaves, but that show little effect on the pattern of vascular development in other parts of the plant (Carland et al., 1999; Deyholos et al., 2000; Koizumi et al., 2000).

Several of the phenotypic characteristics of the *cov1* mutants indicate that the abnormalities might be caused by a defect in auxin signalling. The mutant plants have a stunted growth habit and wrinkled leaves (Fig. 3). Several other mutants defective in auxin signalling and transport also show a dwarf phenotype with wrinkled or curled leaves (Ruegger et al., 1997; Hobbie et al., 2000; Liscum and Reed, 2002). Auxin is known to be involved in controlling cell expansion and has been shown to be involved in regulating hypocotyl elongation in light-grown, but not dark-grown, plants (Jensen et al., 1998; Nakazawa et al., 2001). Given the importance of auxin in all aspects of vascular development, *cov1-1* was examined for its response to auxin (Sachs, 1981; Sachs, 1991; Carland et al., 1999; Sieburth, 1999; Mattsson et al., 1999). Seedlings of *cov1* respond to auxin in a similar manner to wild-type plants. Furthermore, *cov1-1:axr1-3* double mutants behave in a manner similar to the single mutants alone (Fig. 8). Both these lines of evidence suggest that auxin signalling is not the primary defect in *cov1-1*. Direct measurement of auxin levels indicates no difference between mutant and wild type in the upper stem when the vascular defect in *cov1* first becomes apparent. There is a small (twofold) difference in auxin levels at the base of the stem, but this may be a consequence of the altered vascular tissue in *cov1* plants affecting PAT. It is unlikely to account for the vascular patterning defect that is first apparent close to the apex.

According to the canalisation hypothesis (Sachs, 1981; Sachs, 1991), auxin and auxin transport are responsible for the induction of new vascular tissue, and the subsequent draining of auxin from surrounding cells prevents the formation of new vascular strands close to pre-existing vascular bundles. Although there is a vast body of evidence to support the induction and canalisation of the vascular bundles by auxin, the basis of the inhibitory affect is less clear. The *cov1* phenotype is hard to reconcile with this model because a normal pattern

of vascular development is observed but apparently fails to inhibit the formation of additional vascular tissue nearby. The *cov1* phenotype is more consistent with the diffusion-reaction hypothesis in which a second inhibitory component is hypothesised. To date, the nature of this inhibitor has not been identified, but the *cov1* phenotype is consistent with a plant defective in the synthesis, transport or perception of such an inhibitor.

Polyamines are also known to affect cell size and play an important role in internode elongation through cell expansion. The *acl5* mutant, which encodes a spermine synthase, exhibits a short inflorescence stem similar to *cov1-2* (Hanzawa et al., 1997), and, like the *acl5* mutant, the cells in the inflorescence of *cov1-1* plants are much shorter and smaller compared with wild type (data not shown). The *acl5* mutant has much shorter and wrinkled siliques, which is also a characteristic of the *cov1* mutants. *acl5* plants show an increase in vascular tissue within the bundles of the stem, but the spacing and organisation remains relatively similar to the wild type. Polyamines have been hypothesised either to act downstream of auxin signalling or to regulate the interaction of different hormones, such as auxin and gibberellin (Hanzawa et al., 2000). However, the mechanism by which polyamines or their derivatives affect plant development is currently unknown.

The gene responsible for the *cov1* mutation has been cloned by a map-based cloning strategy. Two distinct lines of evidence indicate that the defect is caused by a mutation in the predicted gene At2g20120. First, both mutant alleles can be fully complemented using a fragment containing only this predicted gene. Second, comparison of the *cov1* alleles with the wild-type sequence revealed single base-pair changes within this gene. The complementation analysis was complicated by the fact that the *cov1-1* mutation could be complemented using a fragment that lacked *COV1*. This is explained by fact that *COV1* appears to be part of a very recent tandem duplication event. *COV1* is adjacent to a very closely related gene (termed *LCV1*) that exhibits a 95% amino acid sequence identity with COV1. *LCV1* has a very short promoter region (~500 bp) which it shares with a gene coding for one of the subunits of the 26S proteasome (Fig. 4). Presumably, if the gene is inserted into the genome in a position that increases the expression of *LCV1*, it is sufficiently similar to compensate for *COV1*. Evidence that *LCV1* is not responsible for the *cov1* mutation comes from the fact that no mutation was identified in *LCV1* in either allele of *cov1* and that pGDP1 was only able to partially complement the *cov1-2* allele (68% of plants). The presence of *LCV1* makes it unlikely that either of the *cov1* alleles are functional knockouts, as *LCV1* is expressed at low levels in the plant and was shown to be able to partially complement the mutation.

Both the vascular defect and the growth defects were complemented by pGDP7, which indicates that all the phenotypes associated with *cov1* were a consequence of a defect in a single gene. Expression of the *cov1* gene is high in stems, which is consistent with the observed phenotype. The transcript appears to be alternatively spliced, and a small minority (~1%) of the mRNA retained the second intron. It is unlikely that this change contributes to the mutant phenotype, because the relative increase is small; however, the exact role of the alternative splicing in wild-type plants remains unclear.

COV1 is predicted to be an integral membrane protein of unknown function in plants and a large number of bacteria. The high degree of homology between the genes in plants and bacteria indicates that *COV1* may play an important role in some common pathway, possibly in signalling. Interestingly, the bacterial species that contain the more closely related homologues of COV1 are nearly all species that are associated with plants, including *Mesorhizobium loti* and *Agrobacterium tumefaciens*. Whether these genes are used in the perception or transport of a signal generated in plants remains to be investigated. The *cov1*-mutant phenotype is consistent with that of a plant defective in a component that negatively regulates the differentiation of both xylem and phloem in the developing stem. This component has been predicted in a number of models for vascular development. Further analysis should allow us to determine further the function of *COV1* and how it regulates plant vascular development.

We thank the *Arabidopsis* Biological Resource Centre for the provision of BAC clones and the Nottingham *Arabidopsis* Stock Centre for the provision of seed stocks. We are also grateful to the Kazusa DNA Research Institute for providing cDNA clones and to Malcolm Bennett for the provision of the *IAA2-GUS* construct. This work was supported by the 5th EC Framework Programme within the POPWOOD project.

REFERENCES

Asamizu, E., Nakamura, Y., Sato, S. and Tabata, S. (2000). A large scale analysis of cDNA in Arabidopsis thaliana: generation of 12,028 non-redundant expressed sequence tags from normalized and size-selected cDNA libraries. *DNA Res.* **7**, 175-180.

Bennett, M., Kieber, J., Giraudat, J. and Morris, P. (1998). Hormone regulated development. In *Arabidopsis, Annual Plant Reviews.* Vol. 1 (ed. M. Anderson and J. A. Roberts), pp. 107-150. Sheffield: Sheffield Academic Press.

Bent, A. F. and Clough, S. J. (1998). Agrobacterium germ-line transformation: Transformation of *Arabidopsis* without tissue culture. In *Plant Molecular Biology Manual*. 2nd edn (ed. S. B. Gelvin and R. A. Schilperoot), pp. 1-14. Dordrecht: Kluwer.

Berleth, T. and Mattsson, J. (2000). Vascular development: tracing signals along veins. *Curr. Opin. Plant Biol.* **3**, 406-411.

Carland, F. M., Berg, B. L., FitzGerald, J. N., Jinamornphongs, S., Nelson, T. and Keith, B. (1999). Genetic regulation of vascular tissue patterning in *Arabidopsis*. *Plant Cell* **11**, 2123-2137.

Dengler, N. D. and Kang, J. (2001). Vascular patterning and leaf shape. *Curr. Opin. Plant Biol.* **4**, 50-56.

Deyholos, M. K., Cordner, G., Beebe, D. and Sieburth, L. E. (2000). The *SCAREFACE* gene is required for cotyledon and leaf vein patterning. *Development* **127**, 3205-3213.

Edlund, A., Eklöf, S., Sundburg, B., Moritz, T. and Sandberg, G. (1995). A micro scale technique for gas-chromatography mass-spectrometry measurements of picogram amounts of indole-3-acetic-acid in plant-tissues. *Plant Physiol*. **108**, 1043-1047.

Galweiler, L., Guan, C. H., Muller, A., Wisman, E., Mendgen, K., Yephremov, A. and Palme, K. (1998). Regulation of polar auxin transport by AtPIN1 in *Arabidopsis* vascular tissue. *Science* **282**, 2226-2230.

Guidet, F., Rogowsky, R., Taylor, C., Song, W. and Langridge, P. (1991). Cloning and characterization of a new rye-specific repeat sequence. *Genome* **34**, 81-87.

Hanzawa, Y., Takahashi, T. and Komeda, Y. (1997). *ACL5*: an *Arabidopsis* gene required for internodal elongation after flowering. *Plant J.* **12**, 863-874.

Hanzawa, Y., Takahashi, T., Michael, A. J., Burtin, D., Long, D., Pineiro, M., Coupland, G. and Komeda, Y. (2000). *ACAULIS5*, an *Arabidopsis* gene required for stem elongation, encodes a spermine synthase. *EMBO J.* **19**, 4248-4256.

Hobbie, L., McGovern, M., Hurwitz, L. R., Pierro, A., Yang Liu, N., Bandyopadhyay, A. and Estelle, M. (2000). The *axr6* mutants of

Arabidopsis thaliana define a gene involved in auxin response and early development. *Development* **127**, 23-32.

Jacobs, W. P. (1952). The role of auxin in differentiation of xylem around a wound. *Am. J. Bot*. **39**, 327-337.

Jensen, P., Hangarter, R. P. and Estelle, M. (1998). Auxin transport is required for hypocotyl elongation in light-grown but not dark grown *Arabidopsis*. *Plant Physiol*. **116**, 455-462.

Kepinski, S. and Leyser, O. (2002). Ubiquitination and auxin signalling: a degrading story. *Plant Cell Suppl*. **14**, S80-S95.

Koch, A. J. and Meinhardt, H. (1994). Biological pattern formation: from basic mechanisms to complex structures. *Rev. Mod. Phys*. **66**, 1481-1507.

Koizumi, K., Sugiyama, M. and Fukuda, H. (2000). A series of novel mutants of *Arabidopsis thaliana* that are defective in the formation of continuous vascular network: calling the auxin signal flow canalisation hypothesis into question. *Development* **127**, 3197-3204.

Lincoln, C., Britton, J. H. and Estelle, M. (1990). Growth and development of the *axr1* mutants of *Arabidopsis*. *Plant Cell* **2**, 1071-1080.

Liscum, E. and Reed, J. W. (2002). Genetics of Aux/IAA and ARF action in plant growth and development. *Plant Mol. Biol*. **49**, 387-400.

Mattsson, J., Sung, Z. R. and Berleth, T. (1999). Response of plant vascular systems to auxin transport inhibition. *Development* **126**, 2979-2991.

Nakazawa, M., Yabe, N., Ichikawa, T., Yamamoto, Y., Yoshizumi, T., Hasunuma, K. and Matsui, M. (2001). *DFL1*, an auxin-responsive *GH3* gene homologue, negatively regulates shoot cell elongation and lateral root formation, and positively regulates the light response of hypocotyl length. *Plant J.* **25**, 213-221.

Reinhardt, D., Mandel, T. and Kuhlemeier, C. (2000). Auxin regulates the initiation and radial position of plant lateral organs. *Plant Cell* **12**, 507-518.

Ruegger, M., Dewey, E., Hobbie, L., Brown, D., Bernasconi, P., Turner, J., Muday, G. and Estelle, M. (1997). Reduced naphthylphthalamic acid binding in the *tir3* mutant of *Arabidopsis* is associated with a reduction in polar auxin transport and diverse morphological defects. *Plant Cell* **9**, 745-757.

Sachs, T. (1981). The control of the patterned differentiation of vascular tissues. *Adv. Bot. Res*. **9**, 151-262.

Sachs, T. (1991). The canalisation of vascular differentiation. In *Pattern formation in plant tissues*. pp. 70-87. Cambridge: Cambridge University Press.

Sieburth, L. E. (1999). Auxin is required for leaf vein pattern in *Arabidopsis*. *Plant Physiol*. **121**, 1179-1190.

Steinmann, T., Geldner, N., Grebe, M., Mangold, S., Jackson, C. L., Paris, S., Galweiler, L., Palme, K. and Jurgens, G. (1999). Coordinated polar localization of auxin efflux carrier PIN1 by GNOM ARF GEF. *Science* **286**, 316-318.

Swarup, R., Friml, J., Marchant, A., Ljung, K., Sandberg, G., Palme, K. and Bennett, M. J. (2001). Localization of the auxin permease AUX1 suggests two functionally distinct hormone transport pathways operate in the *Arabidopsis* root apex. *Genes Dev*. **15**, 2648-2653.

Thompson, J. D., Higgins, D. G. and Gibson, T. J. (1994). CLUSTAL-W – Improving the sensitivity of progressive multiple sequence alignment through sequence weighting, position-specific gap penalties and weight matrix choice. *Nucl. Acids Res*. **22**, 4673-4680.

Ye, Z. (2002). Vascular differentiation and pattern formation in plants. *Annu. Rev. Plant Biol*. **53**, 183-202.

Young, B. S. (1953). The effects of leaf primordia on differentiation in the stem. *New Phytol*. **53**, 445-460.

Zhong, R., Taylor, J. J. and Ye, Z. (1999). Transformation of the collateral VB into amphivasal VB in an *Arabidopsis* mutant. *Plant Physiol*. **120**, 53-64.